Atomic-scale study of low-temperature equilibria in iron-rich Al-C-Fe

Rémy Besson* and Alexandre Legris†
Laboratoire de Métallurgie Physique et Génie des Matériaux, CNRS UMR 8517, Université des Sciences et Technologies de Lille, Bâtiment C6, 59655 Villeneuve d'Ascq Cedex, France

Damien Connetable‡ and Philippe Maugis§
CIRIMAT/CNRS UMR 5085 - ENSIACET/INPT, 118 route de Narbonne, 31077 Toulouse, France
(Received 19 November 2007; revised manuscript received 10 June 2008; published 22 July 2008)

The capability of the thermodynamic approach based on the independent point defect approximation to describe low-temperature phase equilibria is investigated and applied to the Al-C-Fe system. The method gives a reasonable description of the multicomponent and multisublattice Fe-rich corner and evidences numerous peculiarities concerning the ordered phases as well as the density-functional-theory (DFT) energy models. The study of Fe_3Al(-C), revealing strong defect-induced instabilities, rules out the LDA, SLDA and GGA schemes and leaves (spin-polarized) SGGA as the only valid one. C stabilizes $L1_2$ Fe_3Al with respect to $D0_3$, which justifies the fcc-type structure of the κ Fe_3AlC compound. The present work also helps in justifying the experimentally observed depletion of C in the κ phase. Finally, a correct description of both Fe_3C and κ requires inclusion of interstitial carbon at low temperature, emphasizing the unexpected importance of interstitial defects in ordered phases.

DOI: 10.1103/PhysRevB.78.014204 PACS number(s): 61.66.Dk, 61.72.J−, 65.40.−b, 31.15.A−

I. INTRODUCTION

The Al-C-Fe system is currently used to create multiphase alloys with controlled mechanical properties at high temperatures. During the thermomechanical elaboration treatments, transient phases appear, among which the κ Fe_3AlC carbide with $E2_1$ structure shows especially intriguing properties. At high temperature (>1000 K), this compound is experimentally known[1] to display a pronounced off-stoichiometry, since it appears in the equilibrium phase diagram only for low C contents ($0.10<x_C<0.15$), which indicates the presence of high amounts of point defects with possibly intricate degrees of order. Besides this experimental study, the Al-C-Fe phase diagram was also calculated[2] through an analysis combining phenomenological thermodynamics and *ab initio* calculations, including evaluations of the energies of selected structures with various compositions. Although these calculations show qualitative agreement with experiment (presence of off-stoichiometry), the calculated composition extent of the κ phase is significantly shrunk to a line compound, a signature of sharp free-energy curves.

The κ compound is thus expected to play a central role in multiphase Al-C-Fe systems, and it would certainly be useful to characterize more accurately its properties, a task that can adequately be performed using atomic-scale approaches. However, the only previous work that tackled this issue, with *ab initio* calculations,[3] was concerned merely with the behavior of the C vacancy in κ. This work showed the strong relaxation of the iron atoms around the defect, inducing a switch from the local environment of $L1_2$ Fe_3Al to that of an iron vacancy in $B2$ FeAl. From these calculations, the authors were able to propose a structural path for the formation of the κ phase from $L1_2$ Fe_3Al. However, due to the free boundary conditions employed, this result could not be used to infer the bulk thermodynamic properties of κ. Apart from this analysis of a particular point defect, no attempt has been made so far toward atomic-scale theoretical investigations of the properties of κ Fe_3AlC.

In order to approach the low-temperature thermodynamic behavior of complex alloys such as Fe_3AlC, it is necessary to have an exhaustive picture of their point defect properties, since the latter are directly connected to the chemical potentials of the species, the knowledge of which is required for realistic modeling. To achieve this, the most general approach would involve the elaboration of a cluster description of the energetics of the compound, suitable for use in either semianalytical (variational method) or numerical (Monte Carlo simulations) equilibrium calculations. The previously mentioned pieces of experimental evidence require the consideration of all kinds of point defects, including vacancies, which implies handling a cumbersome pseudoquaternary Al-C-Fe-vacancy system. Whereas the vast majority of the available cluster analyses have been concerned with binary systems, only a few approaches have tried to extend the procedure to [binary+vacancies].[4,5] Alternatively, an independent point defect analysis constitutes a convenient way to estimate the behavior of ordered compounds. In spite of its limitations (low amounts of defects; hence moderate temperature and off-stoichiometry), better theoretical knowledge of the point defect properties of Fe_3AlC would eventually help in: (i) estimating the trends of the Al-C-Fe system in the iron-rich composition range and (ii) understanding the kinetic paths followed by the system during the elaboration processes and, therefore, the final microstructures.

With the κ compound appearing experimentally at equilibrium with other alloys, a realistic modeling should also encompass the surrounding phases, which justifies investigations extending over the whole Fe-rich corner of the Al-C-Fe system. In this context, the present work is devoted to a detailed atomic-scale analysis of the $T=0$ K energetics of the iron-rich Al-C-Fe system, with special attention paid to κ Fe_3AlC, by means of *ab initio* density-functional calculations coupled with a thermodynamic treatment based on point defects.

As tackling the properties of ternary Al-C-Fe also requires the knowledge of the underlying binary systems, it is worth recalling the amount of work already performed on Al-Fe and C-Fe in the relevant composition domain (iron-rich corner). It is a well-known fact that serious difficulties are encountered when using density-functional theory (DFT) to assess the properties of iron-containing alloys (Fe-Al dilute solid solution; $B2$, $D0_3$, and $L1_2$ ordered compounds).[6] Indeed, some improvement was achieved recently for the $D0_3$ phase through the LDA+U method,[7] but the latter remains confined to specific studies and its inherently higher degree of parameterization makes it uneasy to generalize. As more specifically regards the $D0_3$ and $B2$ compounds, the predicted point defect properties have been shown[7] to depend strongly on the DFT formalism used, with additional intricacy due to the importance of including magnetism. In particular, vacancies in $B2$ FeAl are seemingly better described by spin-polarized local-density approximation (SLDA). However, as will be emphasized in the present work, SLDA can by no means be considered as intrinsically better than spin polarized generalized gradient approximation (SGGA) in any situation. Further investigation is greatly required to estimate the (S)LDA's and (S)GGA's respective merits for iron alloys. (For brevity, we will use the notation (S)LDA (respectively (S)GGA) to refer to both the LDA and SLDA (respectively GGA and SGGA) frameworks.) Regarding the low-temperature $D0_3$ Fe_3Al phase, very few theoretical results are available when compared to those pertaining to $B2$ FeAl. Valuable (in reasonable agreement with experiments) semiquantitative information concerning the point defect formation energies were however provided by DFT calculations without magnetism,[8] which justifies studies (such as the present one) relying on classical DFT approaches without the U term.

Among the identified Fe-C compounds, namely, the solid solution, the $D0_{11}$ Fe_3C cementite, and the $Fe_{10}C$ and Fe_4C phases, only the first two ones were retained in our investigations, since the other carbides show a degree of metastability sufficient for their influence to be neglected in an equilibrium study. Conversely, the metastability of cementite being much lower, it was not reasonable to rule it out *a priori*, all the more since it may be strongly stabilized by ternary additions such as Cr.[9] A DFT (projector-augmented wave PAW–SGGA) analysis of complex point defects in the Fe-C solid solution at moderate temperature (430 K),[10] including defect free energies, showed a considerable binding between C and vacancies. It is also worth mentioning the DFT studies of carbon dissolution and diffusion in ferrite and austenite.[11,12] To our knowledge, however, no atomic-scale study of ordered C-Fe compounds has been performed.

This paper is thus concerned with the low-temperature equilibrium properties of the Al-C-Fe system in the composition domain limited by the following phases: (i) the Fe(-Al,C) solid solution, (ii) the Fe_3Al compound with low amounts of C, (iii) the Al-doped Fe_3C cementite, and (iv) the Fe_3AlC ordered ternary carbide. Although it is the best way to perform this investigation, the exhaustive determination of the convex hull of the system in the whole $[0<(x_{Al},\ x_C)<20\%]$ composition range (as ordinarily done in $T=0$ K cluster studies) would be a task exceedingly long (requiring the determination of an optimal cluster expansion for the pseudoquaternary fcc-based Al-C-Fe-vacancy system) and inherently incomplete, due to the variety of underlying crystallographic structures ($L1_2$, $D0_3$, $D0_{11}$, and κ). Our purpose here is therefore to obtain, at low temperature ($T\simeq 0$ K), relevant information on this pseudoquaternary system via a more tractable point defect analysis [enabling examination of the relative positions of the $H(x_{Al},x_C)$ surfaces], since each such surface around stoichiometry is approximately a linear function of the point defect energies. The present study is thus intended to help in estimating the relative phase stabilities, with particular attention paid to the effect of C and to the possible reasons for the experimental off-stoichiometry of the κ phase. It also provides additional information about the respective merits of the DFT approximations currently used to describe the properties of iron aluminides, these alloys being well known as sources of difficulties in atomic-scale simulations. To this aim, after outlining the relevant methods (Sec. II), a point defect analysis is carried out for each phase in its composition range (Sec. III), yielding the chemical potentials around stoichiometry. The latter are then employed to assess the enthalpies as a function of composition, which eventually allows us to discuss the main low-temperature trends (Sec. IV).

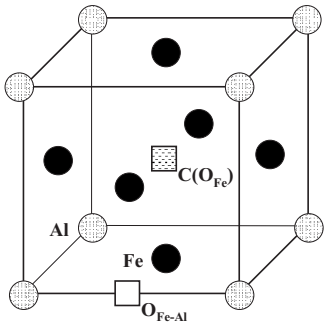

FIG. 1. Unit cell of the Fe_3AlC κ phase, showing both types of interstitial sites O_{Fe} and $O_{Fe\text{-}Al}$ of the $L1_2$ "parent" structure (the former site being fully occupied by C in κ).

II. METHODS

The κ Fe_3AlC phase with $E2_1$ perovskite structure ($CaTiO_3$,$cP5$), of chief interest here, has a unit cell (Fig. 1) that can be viewed as an $L1_2$ Fe_3Al ($AuCu_3$,$cP4$) compound with one supplementary C atom occupying the central site. Its three sublattices thus give rise to nine types of simple point defects (six antisites and three vacancies). In addition, because of the practical importance of interstitial occupancy for carbon in iron-based alloys, the present study takes into account interstitial C in either tetrahedral $\langle\frac{1}{4}\frac{1}{4}\frac{1}{4}\rangle$ or octahedral $\langle\frac{1}{2}00\rangle$ position, the latter labeled as $O_{Fe\text{-}Al}$ below, due to its mixed (four Fe and two Al) neighbor environment. From considerations of atomic size, the possibility of interstitial Al or Fe was neglected. Concerning the $D0_3$ Fe_3Al compound (BiF_3,$cF16$), we respectively labeled as Fe_2 and Fe_3 the mixed Al-Fe and pure Fe cubic sublattices and as $O_{Fe\text{-}Al}$ and O_{Fe} the interstitial octahedral sites located at the centers of

TABLE I. Reference (eV/atom) and GC energies (eV) of point defects in $D0_3$ and $L1_2$ Fe_3Al(-C), calculated in the (S)LDA and (S)GGA frameworks with $1\times1\times1$ (16 atoms) and $2\times2\times2$ (32 atoms) cubic supercells for $D0_3$ and $L1_2$, respectively. In order to further check the convergence and some surprising trends, noted for both compounds with all but the SGGA DFT formalisms, values for antisites pertaining to larger supercells ($2\times2\times2$, 32 atoms, and $3\times3\times3$, 108 atoms, for $D0_3$ and $L1_2$, respectively) are also provided in parentheses (see text).

$D0_3$	Ref.	V_{Al}	Fe_{Al}	V_{Fe_2}	V_{Fe_3}	Al_{Fe_2}	Al_{Fe_3}	C_{Al}	C_{Fe_2}	C_{Fe_3}	$C_{octa_{Fe}}$	$C_{octa_{Fe\text{-}Al}}$
LDA	−8.099	6.726	−3.286 (−3.452)	11.332	10.042	3.299 (3.402)	5.040 (5.139)	−4.122	1.248	1.540	−11.077	−9.792
SLDA	−8.203	7.255	−4.108 (−3.979)	12.061	10.531	3.859 (3.868)	4.941 (5.019)	−2.820	1.895	2.758	−9.789	−8.465
GGA	−7.122	6.184	−2.604 (−2.729)	10.016	8.862	2.696 (2.779)	4.310 (4.394)	−3.273	1.348	1.515	−9.873	−8.716
SGGA	−7.368	6.438	−3.778 (−3.779)	12.314	9.500	4.749 (4.447)	4.559 (4.510)	−1.495	3.433	2.770	−8.758	−5.856
$L1_2$	Ref.	V_{Al}	Fe_{Al}	V_{Fe}		Al_{Fe}		C_{Al}	C_{Fe}		$C_{octa_{Fe}}$	$C_{octa_{Fe\text{-}Al}}$
LDA	−8.034	6.829	−5.822 (−5.766)	10.239		1.440 (−4.731)		−2.739	−1.494		−12.006	−9.763
SLDA	−8.145	7.343	−4.736 (−4.601)	10.617		4.419 (4.467)		−1.993	−0.352		−11.169	−9.160
GGA	−7.057	6.265	−4.920 (−4.876)	9.032		0.861 (−3.788)		−2.040	−1.361		−11.233	−8.745
SGGA	−7.369	6.789	−3.132 (−3.177)	10.056		4.333 (4.336)		−1.075	2.480		−9.172	−7.779

the mixed Fe-Al and pure Fe faces. In the $L1_2$ phase, the C additions were also supposed to be located only at octahedral sites, which in this case can be either of $O_{Fe\text{-}Al}$ or O_{Fe} (six Fe neighbors, site fully occupied in $E2_1$) type.

All defect energies were obtained by *ab initio* calculations performed with the Vienna *Ab initio* Simulation Package (VASP),[13–16] a software that uses plane waves and pseudopotentials in the PAW frame,[17] with the GGA calculations performed with the Perdew-Burke-Ernzerhof (PBE) functional.[18,19] For Fe_3AlC, a supercell containing $2\times2\times2$ unit cells (40 atoms) was used, and the Brillouin zone was sampled with a $6\times6\times6$ Monkhorst-Pack mesh.[20] For Fe_3Al(-C), $2\times2\times2$ ($L1_2$, 32 atoms) and $1\times1\times1$ ($D0_3$, 16 atoms) cubic supercells were used (the k grids contained $6\times6\times6$ and $8\times8\times8$ points, respectively). The validity of the results for these two compounds was checked by additional calculations with larger supercells, namely, $3\times3\times3$ (cubic, 108 atoms) for $L1_2$ and $2\times2\times2$ (trigonal, 32 atoms) for $D0_3$.

As regards $D0_{11}$ Fe_3C(-Al) ($oP16$), we used a $2\times2\times2$ (32 atoms) supercell and a $5\times5\times5$ k sampling. Among the two possible variants for cementite provided by the crystallographic data for intermetallic phases,[21] only the first one—with atomic positions C($4c$) in (890,250,450), Fe_1($4c$) in (036,250,852), and Fe_2($8d$) in (186,063,328)—was considered subsequently, the second variant being found unstable in DFT calculations. The cementite is a rather open structure, suggesting a possible influence of interstitial sites [as noted in other $D0_{11}$ compounds such as $NiAl_3$ (Ref. 22)]. The latter ($4a$ and $4b$ Wyckoff positions) were thus included in our study, this choice being found legitimate *a posteriori* (see below). Finally, for the Fe(-Al,C) solid solution, a $3\times3\times3$ supercell (54 sites) with a $5\times5\times5$ k grid was used. With a plane-wave cut-off energy equal to 500 eV throughout, the previous parameters ensured a 1 meV/atom convergence for all energy values. In order to get a zero local pressure around the defects, all calculations included atomic relaxations together with energy minimization with respect to the supercell size and shape. In magnetic calculations, the ground-state search also allowed the relaxation of spins (including inversion).

The properties of point defects are conveniently described in terms of the so-called grand canonical (GC) quantities, measuring the excess of the property (with respect to the reference undefected system) in a volume surrounding the defect.[23,24] The GC parameters are essentially the thermodynamic extensive variables (namely, the energy, the volume, and the magnetic moment); under the common conditions of zero pressure and magnetic field, the defect-dependent equilibrium properties of a phase depend merely on the GC energies. Therefore, the ground-state point defect structure can be obtained by minimizing the $T=0$ K enthalpy of the system with respect to the point defect numbers at constant composition,[25] the key quantities in this approach being the GC energies of point defects, identical to GC enthalpies under zero pressure, and noted as h_d^s for a defect d on sublattice s:

$$h_d^s = H(N_d^s = 1, N_{\{d'\neq d\}} = 0) - H_0 \tag{1}$$

(H_0 being the enthalpy of the undefected crystal). Under the assumption of independent defects, the $T=0$ K enthalpy of the system containing M unit cells and amounts $\{N_d\}$ of defects of various types d is thus written as

$$H(\{N_d\}) = Mh_0 + \sum_d N_d h_d^s, \tag{2}$$

with h_0 the enthalpy per unit cell for the perfect (undefected) crystal.

III. POINT DEFECTS

A. Defect-induced instabilities in Fe_3Al(-C)

Table I displays the GC point defect energies of Fe_3Al(-C), as obtained in LDA or GGA calculations possibly including spin polarization, together with the reference energies of the undefected supercells. At perfect stoichiometry (no point defect), in agreement with previous calculations,[6] all DFT formalisms predict the stable phase for Fe_3Al to be $D0_3$ except SGGA, for which both structures have almost identical stabilities (within the 1 meV/atom uncertainty of the computational method). The situation is however modi-

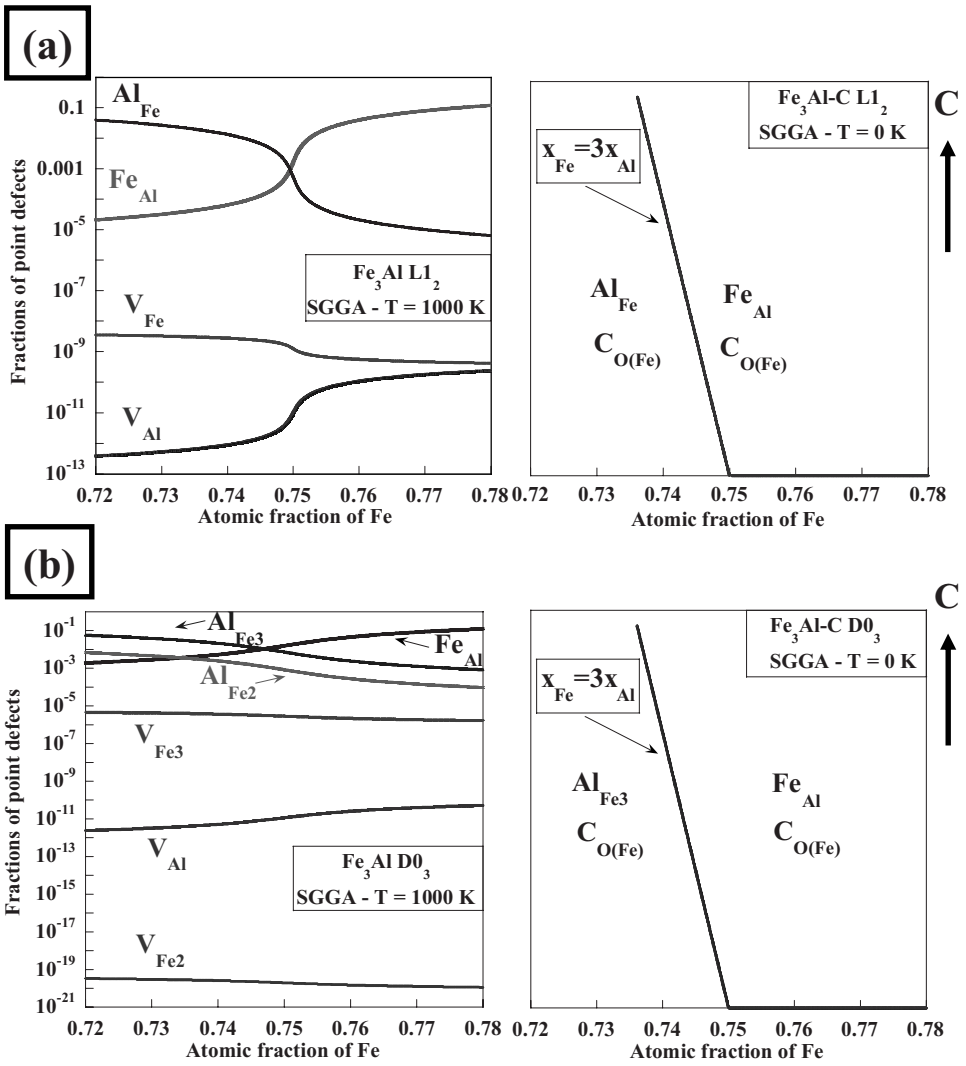

FIG. 2. Point defects for magnetic GGA calculations in (a) $L1_2$ and (b) $D0_3$ Fe_3Al at $T=1000$ K in binary compounds (left figures) and at $T=0$ K including C (right figures). Note that the x axis of each $T=0$ K graph also provides the constituent defects of binary Fe_3Al.

fied significantly by point defects, since the dispersion between the DFT schemes appears to be quite large, a fact that will be found to have important consequences in terms of stability.

The first information that can be inferred from Table I is the point defect structure of each compound around stoichiometry for low temperatures (thus consisting only of structural defects). However, in the $L1_2$ one, achieving these calculations was surprisingly found to be impossible except for the SGGA framework, which solely could yield reasonable results. In all other formalisms, trying to minimize H [relation (2)] led to no solution, this function being unbounded with the numerical values in Table I. The only acceptable $T=0$ K defect structure of $L1_2$ Fe_3Al, obtained from SGGA calculations, is therefore that depicted in Fig. 2(a). The case of $D0_3$ similarly provided no solution in SLDA. Whereas the other three formalisms led to $T=0$ K results according to Fig. 2(b), both the LDA and GGA nonmagnetic calculations for this compound were ruled out by temperature effects (not shown for brevity). These unexpected trends were checked by calculations of antisites in both compounds, using larger supercells (values between parentheses in Table I), which indicated: (i) in $D0_3$ no significant amendment and (ii) for $L1_2$ a strong sensitivity to the supercell size for Al antisites in the nonmagnetic formalisms, which however led to the same unphysical (S)LDA and GGA behavior. The net conclusion is thus, with the inadequacy of the (S)LDA and GGA formalisms for both $D0_3$ and $L1_2$ Fe_3Al, only the SGGA calculations provide a reasonable picture of these compounds around stoichiometry. Note that this conclusion could be reached only by examination of the point defect properties, which proves the importance of including point defects in atomic-scale investigations of intermetallic compounds.

From the underlying linear minimization scheme, it can easily be demonstrated that there exists a relation between these (S)LDA and GGA defect-induced instabilities and the negative (or close to zero) sum of GC enthalpies $h_{\mathrm{Fe}}^{\mathrm{Al}}+h_{\mathrm{Al}}^{\mathrm{Fe}}$ for antisite pairs in these DFT approaches (see Table I). More precisely, the independent point defect framework imposes that $h_{\mathrm{Fe}}^{\mathrm{Al}}+h_{\mathrm{Al}}^{\mathrm{Fe}}$ be positive in order to avoid unphysical behaviors such as spontaneous formation of exceedingly large amounts of antisite defects. In $L1_2$, the trend is already significant in SLDA ($h_{\mathrm{Fe}}^{\mathrm{Al}}+h_{\mathrm{Al}}^{\mathrm{Fe}}\simeq -0.2$ eV) and even more pronounced (<-1 eV) in both nonmagnetic schemes. In $D0_3$, although these values are also slightly positive for nonmagnetic LDA and GGA (considering the favored Fe_2 sublattice), the instability actually arises at any temperature, as confirmed by low-temperature calculations (not displayed for

brevity) showing unrealistic populations of thermal defects. The situation in SLDA is close to that obtained for $L1_2$. Therefore, the SLDA and GGA frameworks equally yield incorrect GC energies for the $D0_3$ phase. These instabilities were suggested, although not pointed out clearly, in a previous study[8] using a nonmagnetic pseudopotential DFT approach with a mixed basis, with the latter work however providing no GC energies but rather formation energies. More recently, a similar situation was found in $B2$ FeCo,[26] with spontaneous formation of antisites at stoichiometry if magnetism is neglected. Such a behavior was also detected in Ni_2Al_3 (Ref. 27): When modeling this compound with an embedded-atom potential,[28] unphysical amounts of interstitial point defects were obtained, whereas correct values were provided by DFT calculations. $L1_2$ Fe_3Al however seems to be more critical, since its defect structure is dramatically sensitive to the DFT approach chosen. Finally, in contrast with previous results concerning $B2$ FeAl,[29] we conclude that point defect calculations for Fe_3Al should therefore be performed in SGGA.

This failure of the (S)LDA and GGA approximations for Fe_3Al is a somewhat surprising result, revealed in the course of the (free-)energy minimization scheme of the compound with respect to its point defect populations. However, one can also get convinced of its validity in a simpler way, merely by considering the stoichiometric case at $T=0$ K. As long as the point defects can be regarded as roughly independent (this is probably true until a few percent of the sites are affected), its enthalpy can be uniformly reduced by creating pairs of antisites (hence at constant composition). This increase in the long-range disorder clearly violates the stability of the ordered structure. Of course, this unphysical process may not lead to complete disorder, since it should be modified when the defects begin to interact. Nevertheless, it is sufficient to demonstrate the inconsistency of the (S)LDA and GGA schemes for the $L1_2$ (and $D0_3$) compound. It should be noted that this unrealistic behavior concerns the spontaneous creation of disorder at constant composition, and it is therefore an intrinsic property (not depending on the overall equilibrium of the compound with the surrounding phases). Such a criterion of long-range-order stability against generation of composition-conserving point defects is quite general and is therefore widely used as a test of the validity of empirical potentials designed for ordered phases (see, for instance, Ref. 30). Its use up to now remains however scarce in the increasing area of *ab initio* calculations about intermetallics. However, such tests would probably be useful, at least for the most common intermetallics (among which are the iron and nickel aluminides).

Finally, the unphysical behavior of antisites in $L1_2$ Fe_3Al obtained in (S)LDA and GGA can be related to a strong tetragonal deformation of the defect supercell around Al_{Fe}, the latter being itself a hint of a structural instability in this compound. Such an instability indeed occurs, as illustrated in Fig. 3 in the GGA case, with the tetragonal Fe_3Al ($c/a \simeq 0.688$) found to be more stable than the cubic $L1_2$ one by more than 0.05 eV/atom, the two variants being separated by a very low–energy barrier (<0.01 eV). On the contrary, in SGGA a tetragonal Fe_3Al unit cell recovers the cubic symmetry, showing that no such transition exists in this framework. Apart from this computational result itself, which should be compared to experiment in order to determine if such a tetragonal structure is really stable, this embodies the possible relation between point defects and structural instabilities.

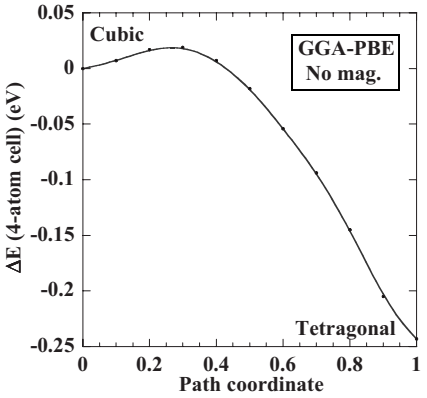

FIG. 3. Energy path from $L1_2$ cubic to tetragonal Fe_3Al (nonmagnetic GGA calculations).

These remarks about stability in Fe_3Al being valid in the absence of C as well, let us now turn specifically toward the effect of this element, the investigation being pursued within the SGGA framework only. It should first be noted (Fig. 2, right) that in both compounds carbon exclusively selects the O_{Fe} octahedral sites, indicating its preference for being surrounded by Fe. In binary Fe_3Al, it is commonly admitted (and confirmed by the phase reference energies in Table I) that, contrary to experiments, the perfect $L1_2$ structure in SGGA is slightly more stable than the $D0_3$ one. By comparison of the $T=0$ K enthalpies [relation (2)], the point defect analysis also makes it possible to go one step further, assessing the influences of off-stoichiometry and carbon addition on the $L1_2/D0_3$ relative stability. Figure 4 displays the corresponding stability domains of the $L1_2$ and $D0_3$ Fe_3Al(-C) phases at $T=0$ K. In the binary compound (no carbon), this indicates that, whereas the $L1_2$ structure is definitely more stable in the Al-rich composition domain, a slight Fe enrichment (less than 2×10^{-3}) reverses the trend in favor of $D0_3$. Since $D0_3$ Fe_3Al is known to accept departures from stoichiometry on both sides ($x_{Al} \simeq 0.22-0.28$), the present result points out that the SGGA formalism for this compound

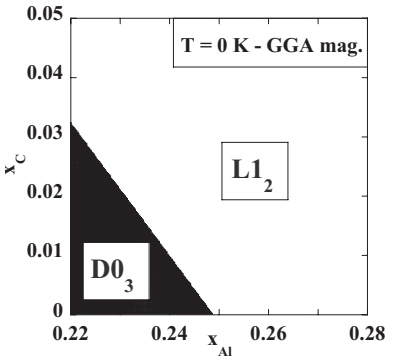

FIG. 4. Stability domains of $L1_2$ and $D0_3$ Fe_3Al(-C) at T $=0$ K according to SGGA calculations.

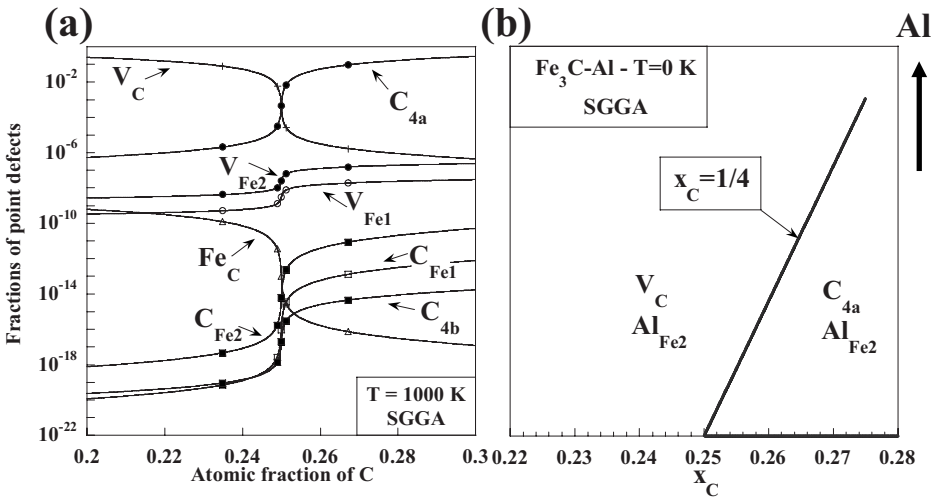

FIG. 5. Point defects in Fe_3C(-Al) (a) at $T=1000$ K in the binary compound and (b) at $T=0$ K including Al (magnetic GGA calculations). Note that the x axis of each $T=0$ K graph also provides the constituent defects of binary Fe_3C.

should be improved in priority on the Al-rich side of stoichiometry. Finally, when C is added, the stability domain of $D0_3$ shrinks, showing the stabilizing effect of this element for $L1_2$. This suggests a C-induced stabilization of the fcc underlying structure and corroborates the preference for such a structure when the C content is increased up to the $E2_1$ phase.

B. Fe_3C(-Al) cementite and Fe(-Al,C) solid solution

The other binary ordered compound of interest in our work is the $D0_{11}$ Fe_3C(-Al) cementite. This phase, known as slightly metastable, must nevertheless be taken into account in practice, due to its easy formation in the various thermomechanical processes. For the present purpose, in a way similar to that obtained for C in the $L1_2/D0_3$ competition in Fe_3Al, we are interested in a possibly stabilizing influence of Al on this phase [guided by the existence of such a influence for Cr (Ref. 9)]. Following the same procedure as the previous one, the point defect structure of Fe_3C(-Al) was therefore determined, and the results are shown in Fig. 5 and Table II. The trends are quite clear, since all DFT formalisms yield similar behaviors (only SGGA is shown). On the whole, Fe_3C(-Al) appears to be a vacancy-type compound on the Fe-rich side of stoichiometry, while C excess is accommodated by $4a$ interstitials. Al preferentially occupies Fe_2 sites, with no influence of the composition ($x_C=1/4$ isoplet). When the temperature rises significantly (for example, $T=1000$ K in Fig. 5), the secondary defects become important for C-rich compositions, whereas the Fe-rich defect structure remains simple, and Fe_3C(-Al) therefore exhibits a dissymetric point defect behavior.

Before turning to the κ compound, let us briefly estimate the properties of the solid solution of Al and C in bcc iron, as the latter will also be used in Sec. IV. Consistency with the previous studies of ordered compounds implies treatment of this system within the independent point defect approximation, and in this framework, only the iron vacancy V_{Fe}, aluminum antisite Al_{Fe}, and octahedral carbon C_{octa} were taken into account, with respective GC enthalpies of 10.460, 3.820, and −8.557 eV (the reference value being $h_0/2=-8.309$ eV/atom). Whatever the composition (low amounts of Al and C), the structural point defects were necessarily Al_{Fe} and C_{octa}; the corresponding $T=0$ K chemical potentials read therefore as

$$\mu_{Al}=\frac{h_0}{2}+h_{Al}^{Fe},\quad \mu_C=h_C^{octa},\quad \mu_{Fe}=\frac{h_0}{2}. \tag{3}$$

C. Interstitials in the κ Fe_3AlC compound

Completing the point defect study, the reference and GC point defect energies for Fe_3AlC, obtained with LDA or GGA calculations including or not including spin polarization, are displayed in Table III. Although all frameworks show qualitative agreement, significant discrepancies occur, mainly for interstitial carbon, vacancies, and Al antisites. As before, no direct conclusion on the stable point defects can be drawn from the GC energies, since the defects are associated with local composition changes that need to be in-

TABLE II. Reference (eV/atom) and GC energies (eV) of point defects in $D0_{11}$ $Fe_3C(-Al)$ cementite, calculated in the (S)LDA and (S)GGA frameworks (32-atom $2\times2\times2$ supercell).

	Ref.	V_{Fe_1}	C_{Fe_1}	V_{Fe_2}	C_{Fe_2}	V_C	Fe_C	Al_{Fe_l}	Al_{Fe_2}	Al_C	C_{4a}	C_{4b}
LDA	−9.566	10.765	2.377	10.871	1.565	10.851	3.392	4.773	4.763	8.434	−9.041	−5.909
SLDA	−9.567	10.717	2.335	10.824	1.534	10.846	3.393	4.774	4.757	8.350	−9.133	−5.972
GGA	−8.396	9.434	2.103	9.484	1.163	9.651	3.339	4.028	4.000	7.529	−8.097	−5.252
SGGA	−8.488	9.980	2.398	9.799	2.037	9.751	3.360	4.460	4.388	9.828	−8.412	−5.762

TABLE III. Reference (eV/atom) and point defect GC energies (eV) in $E2_1$ Fe_3AlC, calculated in the (S)LDA and (S)GGA frameworks (40-atom $2\times2\times2$ supercell).

	Ref.	V_{Al}	Fe_{Al}	C_{Al}	V_{Fe}	Al_{Fe}	C_{Fe}	V_C	Al_C	Fe_C	C_{octa}	C_{tetra}
LDA	−8.726	8.730	−3.522	0.546	10.831	5.731	4.323	11.852	13.223	8.832	−8.920	−6.676
SLDA	−8.733	8.412	−3.268	0.612	10.806	5.742	4.117	11.380	13.036	8.893	−8.742	−6.597
GGA	−7.718	7.764	−2.863	0.950	9.563	5.012	3.966	10.684	12.101	8.494	−7.831	−5.762
SGGA	−7.743	6.593	−2.120	1.655	9.466	5.223	3.369	10.750	11.501	7.835	−7.211	−5.818

cluded globally in the analytic treatment [Eq. (2)]. Table III nevertheless shows the marked preference of C for octahedral sites, since $E_{GC}(C_{octa})-E_{GC}(C_{tetra})\simeq-2$ eV whatever the DFT framework used. As regards the $T=0$ K point defect structure, the minimization procedure naturally yields zone limits of two types: $x_i=1/5$ or 3/5 and $x_i=3x_j$ (with i, j=Al, Fe, or C), corresponding to sharp changes in the point defect nature, a well-known effect in ordered compounds, possibly inducing drastic changes in the properties for slight composition changes. This effect, already noted for additions in binary ordered systems, is also present in intrinsically ternary ones. The role of interstitial C in the compound is not easy to infer intuitively. From a crystallographic point of view, both the central and the octahedral interstitial positions in Fe_3AlC are octahedral sites, the difference merely lying in the chemical nature of the neighboring atoms [pure Fe and mixed (Fe,Al), respectively]. As pointed out in Ref. 1, systematic studies of T_3MC compounds (with T=transition metal and M=metal$\neq T$) indicated that C occupies only pure Fe octahedra, its insertion into a mixed octahedron leading to an energetically unfavorable distortion. Such a hypothesis, conceiving the perovskite as a binary Fe-Al alloy with *a posteriori* additions of C, provides an estimation of the C solubility limit, related to the number of available Fe octahedra in the Fe-Al underlying structure. It cannot however be rigorously justified, since the equilibrium phase structure results from a unique global energy minimization for the ternary compound (in equilibrium with other candidate phases) with respect to its internal variables. On the whole, there exists no convincing argument to justify interstitials being neglected *a priori* in the κ phase nor as regards the respective roles of octahedral and tetrahedral sites.

However, in order to evaluate explicitly the sensitivity of the results to interstitial C, it is instructive to perform at first an "interstitial-free" calculation of the $T=0$ K point defect structure. Figures 6(a) and 6(b) show the conclusions of such a calculation: Neglecting interstitial C leads to somewhat dispersed results, the SGGA here again behaving differently from the other frameworks. The ambiguity occurs essentially in the composition domain corresponding to $x_{Al}<1/5$ and $x_C>1/5$, with SGGA yielding Al vacancies and a $x_{Fe}=3x_C$ zone limit, whereas all other calculations clearly point out C_{Al} defects with a $x_{Fe}=3/5$ limit. Thus, although the C-depleted off-stoichiometry is, whatever the DFT formalism, coherently predicted to be accommodated by Al_{Fe}, Fe_{Al}, C_{Fe}, and V_C (with changes at $x_{Fe}=3x_{Al}$, $x_{Al}=1/5$, and $x_C=1/5$), disagreement between the DFT formalisms occurs in the C-rich part of the composition diagram.

Including interstitial C (in octahedral sites) dramatically clarifies the situation [Fig. 6(c)], the $T=0$ K point defect structure being depicted then more coherently: Only four composition domains appear, delimited by the $x_{Fe}=3x_{Al}$ and $x_C=1/5$ isoplets, and the off-stoichiometry leads to Al_{Fe}, Fe_{Al}, V_C, and C_{octa} point defects. This clearly shows the importance of including interstitial C (in octahedral sites) to ensure a proper description of Fe_3AlC. At moderate temperature, the latter should thus be modeled reasonably using a four-defect model with the formula $(Fe,Al)_3(Al,Fe)$ (C,vacancy) (C_{octa}), refining the currently used three-sublattice description of κ. In the present case, due to the relative simplicity of the cubic underlying crystallographic structure, the role of interstitial C could perhaps have been expected from intuitive arguments. However, other cases (for example, Fe_3C) may be encountered for which no such heuristic guidelines exist, and a correct initial defect identification would then be critical.

The knowledge of the $T=0$ K point defects in each phase and each composition domain eventually makes it possible to estimate analytically the low-temperature chemical potentials of the three elements, which show quite different behaviors (Table IV). In both Fe_3Al(-C) structures, the C chemical potential is independent of the composition (being simply equal to the GC energy of the interstitial defect), whereas this parameter has an influence on the potentials of both other (intrinsic) elements. In cementite, a similar behavior is noticed for the intrinsic chemical potentials, together with that of Al, which is sensitive to the composition (due to its substitutional occupancy). In κ Fe_3AlC, the C chemical potential is

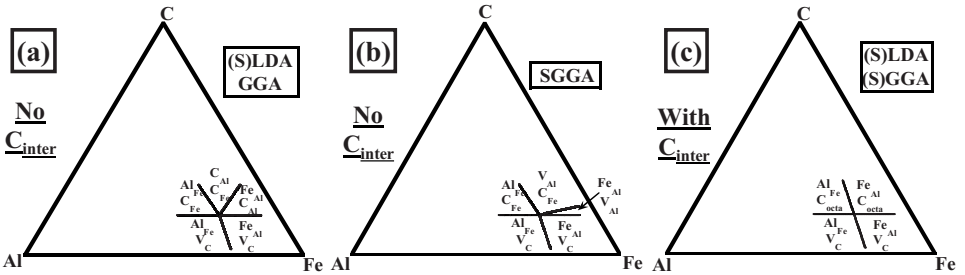

FIG. 6. $T=0$ K domains of stability of point defects in Fe_3AlC as a function of the DFT formalism used, with (a) and (b) neglecting and (c) including the octahedral occupancy for C.

TABLE IV. Chemical potentials at $T=0$ K in Fe_3Al(-C) ($D0_3$ and $L1_2$), Fe_3C(-Al) and Fe_3AlC, calculated in the SGGA framework.

Phase	Composition range	μ_{Al}	μ_C	μ_{Fe}
$D0_3$ Fe_3Al(-C)	$x_{Al}<x_{Fe}/3$	$h_0/16-3/4h_{Fe}^{Al}$	$h_C^{O_{Fe}}$	$h_0/16+h_{Fe}^{Al}/4$
	$x_{Al}>x_{Fe}/3$	$h_0/16+3/4h_{Al}^{Fe_3}$	$h_C^{O_{Fe}}$	$h_0/16-h_{Al}^{Fe_3}/4$
$L1_2$ Fe_3Al(-C)	$x_{Al}<x_{Fe}/3$	$(h_0-3h_{Fe}^{Al})/4$	$h_C^{O_{Fe}}$	$(h_0+h_{Fe}^{Al})/4$
	$x_{Al}>x_{Fe}/3$	$(h_0+3h_{Al}^{Fe})/4$	$h_C^{O_{Fe}}$	$(h_0-h_{Al}^{Fe})/4$
$D0_{11}$ Fe_3C(-Al)	$x_C>1/4$	$h_0/12-h_C^{4a}/3+h_{Al}^{Fe_2}$	h_C^{4a}	$h_0/12-h_C^{4a}/3$
	$x_C<1/4$	$h_0/12+h_V^C/3+h_{Al}^{Fe_2}$	$-h_V^C$	$h_0/12+h_V^C/3$
$E2_1$ Fe_3AlC	$x_C>1/5;\quad x_{Al}<x_{Fe}/3$	$(h_0-3h_{Fe}^{Al}-h_C^i)/4$	h_C^i	$(h_0+h_{Fe}^{Al}-h_C^i)/4$
	$x_C>1/5;\quad x_{Al}>x_{Fe}/3$	$(h_0+3h_{Al}^{Fe}-h_C^i)/4$	h_C^i	$(h_0-h_{Al}^{Fe}-h_C^i)/4$
	$x_C<1/5;\quad x_{Al}>x_{Fe}/3$	$(h_0+3h_{Al}^{Fe}+h_V^C)/4$	$-h_V^C$	$(h_0-h_{Al}^{Fe}+h_V^C)/4$
	$x_C<1/5;\quad x_{Al}<x_{Fe}/3$	$(h_0-3h_{Fe}^{Al}+h_V^C)/4$	$-h_V^C$	$(h_0+h_{Fe}^{Al}+h_V^C)/4$

sensitive only to the atomic fraction of this element, while those of both other elements show a more complex behavior and vary when crossing each zone limit. These analytic expressions for the chemical potentials will be used in Sec. IV, enabling numerical estimations of the low-temperature enthalpy per atom $H_{at}=\Sigma_i x_i\mu_i$ of the phases in each composition domain.

Finally, since the GC energies and chemical potentials together give access to the defect formation energies (more readily comparable with experiments) at $T=0$ K, the latter quantities are also provided in Table V (in the SGGA scheme) for the ordered compounds considered in the present work [namely, $D0_3$ and $L1_2$ Fe_3Al-C, $D0_{11}$ Fe_3C-Al, and $E2_1$ Fe_3AlC]. As expected, the structural defects in each relevant composition domain have zero formation energies, and those with low positive values should be formed easily by thermal activation. Also note the large values occurring in Fe_3AlC, which recall those obtained in nonmetallic systems (oxides, etc.).

IV. LOW-TEMPERATURE ANALYSIS OF THE Al-C-Fe SYSTEM

Relying on the previous point defect studies, we then proceed to an analysis of the possible low-temperature equilibria between these phases. First of all, it should be recalled that the previous conclusions exclude the use of any formalism except SGGA. The latter will consequently constitute the only framework of the following discussion, but this does not dismiss the other formalisms which may perform better than the SGGA in some cases (for instance, SLDA in perfect Fe_3Al). In fact, it might also be conceivable to devise mixed (S)LDA/(S)GGA schemes, using distinct DFT calculations for the different phases. However, we did not retain such a procedure, by reason of its significant level of arbitrariness and also because it obviously precludes any assessment of the merits of a single DFT framework.

In Ref. 2, the $L1_2$ and $E2_1$ compounds were simultaneously treated as a continuous solution of C, and the switch-

TABLE V. $T=0$ K point defect formation energies (eV) in the ordered compounds encountered in this work (SGGA framework throughout).

$D0_3$ Fe_3Al-C	V_{Al}	Fe_{Al}	V_{Fe_2}	V_{Fe_3}	Al_{Fe_2}	Al_{Fe_3}	C_{Al}	C_{Fe_2}	C_{Fe_3}	$C_{octa_{Fe}}$	$C_{octa_{Fe\text{-}Al}}$
$x_{Al}<x_{Fe}/3$	1.904	0	4.002	1.188	0.971	0.781	2.729	3.879	3.216	0	2.902
$x_{Al}>x_{Fe}/3$	2.489	0.781	3.806	0.992	0.190	0	3.314	3.683	3.020	0	2.902
$L1_2$ Fe_3Al-C	V_{Al}	Fe_{Al}	V_{Fe}		Al_{Fe}		C_{Al}	C_{Fe}	$C_{octa_{Fe}}$		$C_{octa_{Fe\text{-}Al}}$
$x_{Al}<x_{Fe}/3$	1.769	0	1.904		1.201		3.077	3.500	0		1.393
$x_{Al}>x_{Fe}/3$	2.670	1.201	1.604		0		3.978	3.200	0		1.393
$D0_{11}$ Fe_3C-Al	V_{Fe_1}	C_{Fe_1}	V_{Fe_2}	C_{Fe_2}	V_C	Fe_C	Al_{Fe_1}	Al_{Fe_2}	Al_C	C_{4a}	C_{4b}
$x_C>1/4$	1.467	2.297	1.286	1.936	1.339	3.461	0.072	0	5.541	0	2.650
$x_C<1/4$	1.913	4.082	1.732	3.721	0	1.676	0.072	0	3.756	1.339	3.989
$E2_1$ Fe_3AlC	V_{Al}	Fe_{Al}	C_{Al}	V_{Fe}	Al_{Fe}	C_{Fe}	V_C	Al_C	Fe_C	C_{octa}	C_{tetra}
$x_C<1/5;\ x_{Al}<x_{Fe}/3$	1.191	0	7.003	1.944	3.103	6.597	0	6.153	4.607	3.539	4.932
$x_C<1/5;\ x_{Al}>x_{Fe}/3$	3.519	3.103	9.331	1.169	0	5.822	0	3.826	5.383	3.539	4.932
$x_C>1/5;\ x_{Al}<x_{Fe}/3$	0.306	0	2.580	1.060	3.103	2.174	3.539	10.577	9.031	0	1.393
$x_C>1/5;\ x_{Al}>x_{Fe}/3$	2.634	3.103	4.907	0.284	0	1.398	3.539	8.249	9.806	0	1.393

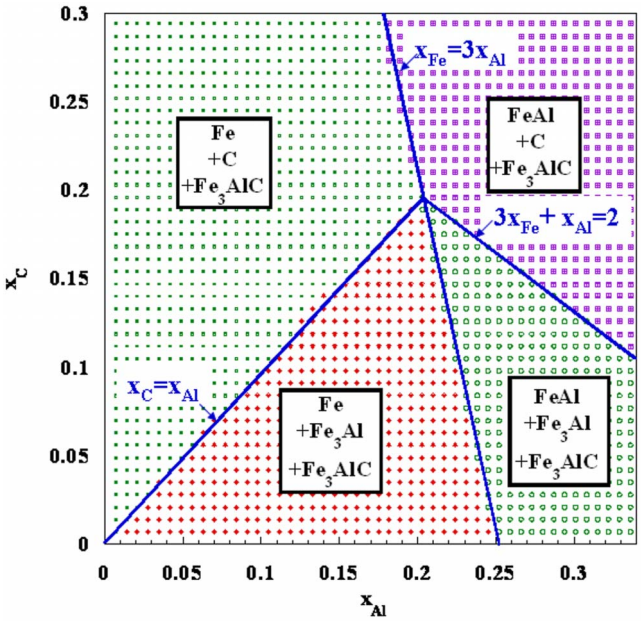

FIG. 7. (Color online) Stability domains of three-phase systems involving stoichiometric compounds at $T=0$ K (magnetic GGA calculations).

ing from one phase to the other therefore was supposed to occur by progressive filling of the O_{Fe} and then $O_{Fe\text{-}Al}$ interstitial sites. Confirmation of this "monotonic" mode of filling would require methods far beyond the scope of this work such as, for example, by cluster approaches modeling of carbon in (O_{Fe}; $O_{Fe\text{-}Al}$) sites, the underlying $L1_2$ Fe_3Al structure being considered as fixed (no point defect and disorder). The present investigation, concerning the properties around stoichiometry, cannot therefore give information about the evolution of the behavior of C when going from Fe_3Al(-C) to Fe_3AlC. It may however help to understand a surprising feature of Fe_3AlC, namely, the phase separation $Fe_3AlC \rightarrow Fe_3AlC_{1-x}+C_{graphite}$, reflected by the experimental maximum C solubility of 15% at 1000 K.[1]

Using the present methodology, assessing the effect of off-stoichiometry cannot be undertaken directly, due to the nonderivability of the enthalpies (as a function of composition) at $T=0$ K, which prevents application of the usual rule of common tangent planes. This difficulty can be overcome by means of a two-step analysis, the first of which consists in determining the "stoichiometric convex hull" associated with the phases considered, namely, the $H_{stoichio}(x_{Al},x_C)$ function obtained under the hypothesis of perfectly stoichiometric line compounds. Within this hypothesis (no off-stoichiometry allowed), each composition domain contains (for a ternary system) three phases, since the emergence of single- and double-phased domains is a consequence of the possibility of departures from stoichiometry. Besides $D0_3$ and $L1_2$ Fe_3Al(-C), $D0_{11}$ Fe_3C(-Al), $E2_1$ Fe_3AlC, and Fe(-Al,C) (solid solution), the application of this procedure to Al-C-Fe requires taking into account graphite C and $B2$ FeAl in order to ensure a bounded behavior in the composition domain around κ. For $B2$ FeAl, the value $h_0=-6.359$ eV/atom (obtained from SGGA calculations) was used. As regards graphite, owing to the doubtful value provided by DFT, its energy was calculated by adding the experimental difference $E(C_{diamond})-E(C_{graphite})=19.8$ meV/atom to the DFT values obtained for diamond, yielding $E(C_{graphite})=-9.112$ eV/atom for (S)GGA. The ideal stoichiometric stability diagram is presented in Fig. 7, showing only three-phase domains. Cementite never appears, in agreement with its metastable character (the influence of point defects on this conclusion will be considered below).

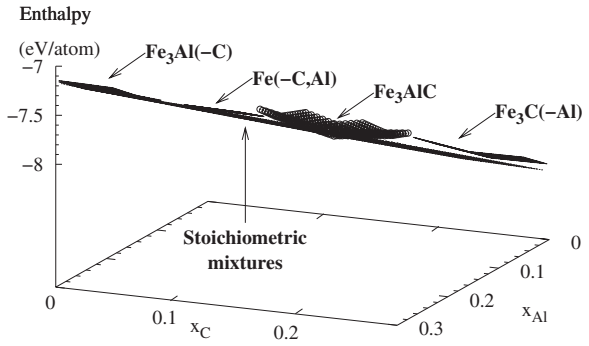

FIG. 8. $T=0$ K enthalpy-composition diagram for the phases considered in this work (bcc, $L1_2$, $D0_3$, $D0_{11}$, and $E2_1$), together with the enthalpy of the mixtures of the three stoichiometric phases (stoichiometric convex hull) corresponding to Fig. 7 (magnetic GGA calculations).

The effect of off-stoichiometry is examined in the second step, by superposing onto $H_{stoichio}$ the ($H_{at}=x_i\mu_i$) surfaces of the phases obtained via the previously described point defect analysis, which requires the chemical potentials of Fe_3Al(-C), Fe_3C(-Al), and Fe_3AlC (Table IV). Figure 8 displays the convex hull of the three-phase stoichiometric mixtures (exhibiting an almost flat shape), together with the superposition of these nonstoichiometric compounds. The sharpest slopes are associated with Fe_3AlC, which suggests a poor accommodation of off-stoichiometry (at least for low temperature) and, hence, a marked trend to phase separation. On the contrary, the enthalpy surfaces associated with Fe_3Al(-C) and the solid solution have wider shapes, indicating the possible opening of single- and double-phased do-

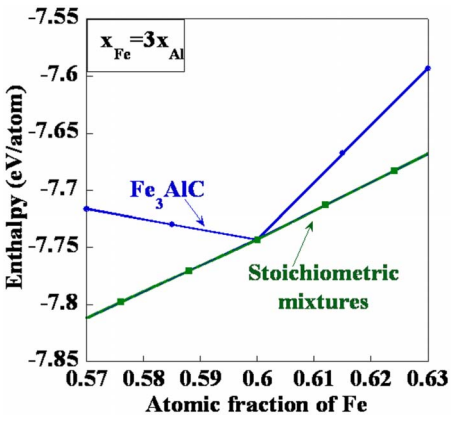

FIG. 9. (Color online) Cut of the $T=0$ K enthalpy-composition diagram in Fig. 8 along the $x_{Fe}=3x_{Al}$ line, for comparison of the stoichiometric mixtures and $E2_1$ Fe_3AlC.

mains when T increases, and cementite shows an intermediate behavior, with similar slopes for C depletion and excess. Our results also provide a rough interpretation of the experimental dissymetric behavior of κ (according to whether $x_C < 0.2$ or not) by considering the influence of the C content on the relative positions of $H_{stoichio}$ and H_κ. Figure 9, which corresponds to a cut of Fig. 8 along the $x_{Fe}=3x_{Al}$ line, thus indicates that $H_\kappa - H_{stoichio}$ is larger for $x_{Fe} < 0.6$ (that is, for $x_C > 0.2$), which is coherent with a poorer accommodation of off-stoichiometry and, thus, an increased trend to unmixing in this composition domain. In agreement with experimental conclusions, κ therefore appears as preferentially understoichiometric in C, even at low temperature.

Finally, the question arises as to whether this phenomenon is related to interstitial C. As already noted in Fig. 6, the role of interstitials is limited to the C-rich domain, which implies that for $x_C < 1/5$ the κ enthalpies with and without interstitial C are identical. Moreover, for $x_C > 1/5$ the interstitial-free curve is necessarily above that with interstitial (since the latter structure is the most stable one). It follows that neglecting interstitial C should lead to the same conclusion as regards phase separation. This may partly explain why three-sublattice (hence ignoring interstitial C) approaches may succeed in predicting such a trend.[2]

V. CONCLUSION

The thermodynamic properties of complex alloys and their equilibria strongly depend on their point defects, which constitute the elementary low-temperature excitations governing the free energy. The energetics of these defects can be conveniently obtained using the available *ab initio* methods, which now offer the possibility of tackling multiconstituent and multistructured mixtures provided a tractable thermodynamic framework is employed. The independent point defect approximation used here seems to be well designed for this task, since the present study has demonstrated its capability of yielding realistic trends for Al-C-Fe; several major results obtained this way are worth emphasizing.

First, only the SGGA point defect calculations give correct results for $L1_2/D0_3$ Fe_3Al, since all other formalisms entail an unstable $L1_2$ phase with respect to antisite defect formation. This behavior is probably related to the strong structural relaxation around Al_{Fe} that can be traced back to the existence of a tetragonal phase predicted to be more stable than the cubic one. Carbon stabilizes the $L1_2$ structure, suggesting the existence of a continuous connection between the $L1_2$ Fe_3Al(-C) solid solution and the κ phase; this may help to understand why Fe_3AlC has an $L1_2$ rather than a $D0_3$ related structure.

The study of relative stability between $D0_3$ and $L1_2$ Fe_3Al(-C) points out the intrinsic difficulties of the DFT methods in describing the Fe-Al system. These particular phases and their point defect properties may constitute a benchmark to check possible improvements in electronic structure calculations. The point defect study of the various phases investigated also evidences the importance of taking into account interstitial carbon in Fe_3C and Fe_3AlC in describing carbon-rich phases, although such phases may not appear in the equilibrium phase diagram.

By constructing $H_{stoichio}$, the stoichiometric convex hull associated with the considered phases allows us to draw a $T=0$ K phase diagram made of three-phase coexistence domains. A cut of the enthalpy surfaces displays trends that indicate that the Fe_3AlC kappa compound should be carbon depleted at equilibrium, as experimentally observed. The shapes of the enthalpy-composition surfaces are quite different: flat for Fe_3Al(-C) and Fe(-Al,C), intermediate for Fe_3C(-Al), and sharp for Fe_3AlC.

To summarize, beyond the particular case presented here, we more generally believe that the thermodynamic analysis relying on the independent point defect approximation is a powerful tool in spite of its simplicity. It allows handling multicomponent phases with general crystallographic structures. It therefore constitutes a soundly based and convenient approach to address thermodynamics at the atomic scale, before possibly resorting to more powerful but much heavier methods.

*Author to whom correspondence should be addressed; remy.besson@univ-lille1.fr
†alexandre.legris@univ-lille1.fr
‡damien.connetable@ensiacet.fr
§philippe.maugis@ensiacet.fr

[1] M. Palm and G. Inden, Intermetallics **3**, 443 (1995).
[2] H. Ohtani, M. Yamano, and M. Hasebe, IEEE Trans. Compon., Hybrids, Manuf. Technol. **44**, 1738 (2004).
[3] B. V. Reddy and S. C. Deevi, Mater. Sci. Eng., A **329-331**, 395 (2002).
[4] F. Lechermann and M. Fahnle, Phys. Rev. B **63**, 012104 (2000).
[5] A. Van der Ven and G. Ceder, Phys. Rev. B **71**, 054102 (2005).
[6] F. Lechermann, F. Welsch, C. Elsasser, C. Ederer, M. Fahnle, J. M. Sanchez, and B. Meyer, Phys. Rev. B **65**, 132104 (2002).
[7] F. Lechermann, M. Fahnle, B. Meyer, and C. Elsasser, Phys. Rev. B **69**, 165116 (2004).
[8] J. Mayer, B. Meyer, J. S. Oehrens, G. Bester, N. Bornsen, and M. Fahnle, Intermetallics **5**, 597 (1997).
[9] *Phase Equilibria in Iron Ternary Alloys*, edited by G. V. Raynor and V. G. Rivlin (Institute of Metals, London, 1988).
[10] C. J. Forst, J. Slycke, K. J. Van Vliet, and S. Yip, Phys. Rev. Lett. **96**, 175501 (2006).
[11] D. E. Jiang and E. A. Carter, Phys. Rev. B **67**, 214103 (2003).
[12] C. Domain, C. S. Becquart, and J. Foct, Phys. Rev. B **69**, 144112 (2004).
[13] G. Kresse and J. Hafner, Phys. Rev. B **47**, 558 (1993).
[14] G. Kresse and J. Hafner, Phys. Rev. B **49**, 14251 (1994).
[15] G. Kresse and J. Furthmüller, Phys. Rev. B **54**, 11169 (1996).
[16] G. Kresse and J. Furthmüller, Comput. Mater. Sci. **6**, 15 (1996).
[17] G. Kresse and D. Joubert, Phys. Rev. B **59**, 1758 (1999).
[18] J. P. Perdew, K. Burke, and M. Ernzerhof, Phys. Rev. Lett. **77**, 3865 (1996).

[19] J. P. Perdew, K. Burke, and M. Ernzerhof, Phys. Rev. Lett. **78**, 1396 (1997).
[20] H. J. Monkhorst and J. D. Pack, Phys. Rev. B **13**, 5188 (1976).
[21] P. Villars and L. Calvert, *Pearson's Handbook of Crystallographic Data for Intermetallic Phases*, 2nd ed. (ASM International, Metals Park, OH, 1991).
[22] M. Rasamny, M. Weinert, G. W. Fernando, and R. E. Watson, Phys. Rev. B **64**, 144107 (2001).
[23] J. Mayer, C. Elsasser, and M. Fahnle, Phys. Status Solidi B **191**, 283 (1995).
[24] B. Meyer and M. Fahnle, Phys. Rev. B **59**, 6072 (1999).
[25] R. Besson, A. Legris, and J. Morillo, Phys. Rev. Lett. **89**, 225502 (2002).
[26] M. Neumayer and M. Fahnle, Phys. Rev. B **64**, 132102 (2001).
[27] D. Tingaud, Ph.D. thesis, Université de Limoges, 2006.
[28] Y. Mishin, M. J. Mehl, and D. A. Papaconstantopoulos, Phys. Rev. B **65**, 224114 (2002).
[29] R. Besson, A. Legris, and J. Morillo, Phys. Rev. B **74**, 094103 (2006).
[30] D. O. Welch, G. J. Dienes, O. W. Lazareth, and R. D. Hatcher, J. Phys. Chem. Solids **45**, 1225 (1984).